THE JOURNAL OF PHYSICAL CHEMISTRY C

Article

pubs.acs.org/JPCC

Seeded Growth Synthesis of Composition and Size-Controlled Gold–Silver Alloy Nanoparticles

David Rioux and Michel Meunier*

Laser Processing and Plasmonics Laboratory, Department of Engineering Physics, Polytechnique Montréal, C.P. 6079, Succ. Centre-ville, Montréal, Québec H3C 3A7, Canada

Supporting Information

ABSTRACT: We propose a novel methodology to synthesize monodisperse gold–silver alloy nanoparticles (NPs) with fine control of size and composition. The synthesis is based on a combination of the coreduction of gold and silver salts for the formation of alloys and the seeded growth approach for the formation of size-controlled NPs. While the simple use of coreduction gives alloy NPs limited to ∼30 nm, the combination of both methods yields spherical alloy NPs with a size that can be controlled between ∼30 and ∼150 nm, with a coefficient of variation smaller than 15%. The alloy NPs can be synthesized to any composition between pure silver and pure gold. We also show that the alloy composition is non-homogeneous, with a gold-rich core and a silver-rich surface. The transition in the alloy composition is gradual from the core to the surface, resulting in optical properties very similar to the optical properties of a homogeneous alloy, except for the smaller (∼30 nm) NPs. A multilayer Mie model has been introduced to study the effect of the nonhomogeneous alloy profile on the optical properties of the NPs. The inhomogeneous alloy structure is likely caused by galvanic replacement of Ag atoms at the surface by Au ions during the growth of the NPs.

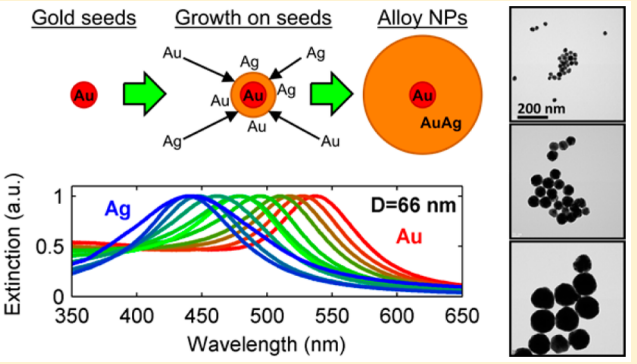

INTRODUCTION

In recent years, the field of plasmonics has been flourishing with new advances and discoveries. There has been tremendous development on new geometries for nanoparticles (NPs) or for nanostructured surfaces in order to control the optical properties or obtain new functionalities.[1−4] Surprisingly, the development in terms of material used for these nanostructures has been much more limited as most applications of plasmonics use either gold (Au) or silver (Ag). These two metals have the best plasmonic resonance, and although Ag has better plasmonic properties,[2] Au is biocompatible and has a better stability and resistance to oxidation, making it a better candidate for several applications.[5] In either case, the control of the optical properties of the plasmonic nanomaterials can only be obtained through a fine control of the geometry using, for instance, nanorods, nanotriangles, or nanoshells rather than spherical NPs. However, the optical properties are generally very sensitive to the shape of the NPs,[3] making it crucial to obtain suspensions with extremely good uniformity in size and shape. Therefore, it would be interesting to keep spherical NPs and to control their optical properties by changing the material composition instead of the shape. Because Au and Ag are the best plasmonic metals available, their alloys are a logical choice for a new material. Gold–silver (AuAg) alloy nanoparticles (ANPs) are very interesting because their plasmonic resonance peak can be tuned with the alloy composition.[6]

Synthesis of AuAg ANPs has been reported by ultrasonic alloying of Au and Ag NPs,[7] by laser alloying of Au and Ag NPs,[6,8] by laser ablation of a solid AuAg alloy target,[5,9] by photochemical coreduction of Au and Ag salts,[10] or by using conventional chemical reduction methods in organic solvents[11−13] or aqueous solutions.[14−19] In every case, the plasmon peak position was found to vary almost linearly with alloy composition. However, none of these approaches have demonstrated the synthesis of ANPs with a controlled size, and these ANPs are smaller than 30 nm in diameter. In plasmonic applications, large particles (>50 nm) are often needed in order to benefit from their high scattering efficiency. For example, suitably large AuAg ANPs with different compositions can act as chromatic biomarkers in biomedical imaging.[20−22]

This paper describes the synthesis of composition and size-controlled AuAg ANPs by seeded growth through the chemical reduction approach. To our knowledge it is the first time that the formation of size-controlled AuAg ANPs is demonstrated for sizes larger than 30 nm. The paper also studies the homogeneity of the alloy composition and its effect on the optical properties of the ANPs.

Received: March 20, 2015
Revised: May 12, 2015

DOI: 10.1021/acs.jpcc.5b02728
J. Phys. Chem. C XXXX, XXX, XXX−XXX

Chemical Synthesis of Plasmonic NPs. Of all the aforementioned approaches for NP synthesis, the simplest is the chemical reduction, which is based on the reduction of a metal salt transforming the metallic ions into neutral atoms. The low solubility of these free atoms induces their fast nucleation into small metallic clusters, and the remaining neutral atoms then grow on the existing particles. The most famous example of such chemical synthesis for Au NPs is the Turkevich method, where the NPs are formed through reduction of chloroauric acid with sodium citrate in water.[23] In the Turkevich approach, the size of the NPs can be controlled by changing the ratio of Au to citrate during synthesis.[24,25] For small sizes, this approach yields NPs with a coefficient of variation (CV, defined as the standard deviation of the size distribution divided by the mean size) lower than 10%, which corresponds to excellent monodispersity. However, the dispersion in size and shape is much worse when producing large (>40 nm) NPs.

The most crucial aspect for the synthesis of monodispersed NPs is the temporal separation of nucleation and growth steps during the NP formation. This has been achieved for both pure Au and pure Ag NPs by using the seeded growth approach which consists of first forming small monodispersed NPs (for example, using the Turkevich approach) and then using them as seeds for the growth of larger NPs. It is important to prevent the formation of new seeds during the growth step. This is achieved by carefully controlling the growth conditions and choosing the appropriate reducing agent. For example, a reducing agent that preferably reduces the ions in the presence of a metallic surface at low temperature will prevent new nucleation.[26−28] Even if the seeded growth approach has been successfully used to synthesize large and size-controlled Au and Ag NPs, this approach has not been shown for AuAg ANPs.

Producing ANPs requires a simultaneous reduction of two or more metal salts. The final composition of the NPs is determined by the initial ratio of the metal salts. However, the different nature of the metal salts can affect the reaction rates or even interfere with each other. For instance, this is the case between silver nitrate ($AgNO_3$) and chloroauric acid ($HAuCl_4$); if their concentrations are too high, the chlorine ions from the Au salt combine with the Ag ions and produce silver chloride, which precipitates and cannot contribute to particle growth. This precipitation reaction limits the concentration of metal salts that can be used, therefore limiting the final NP concentration.[16]

We found that it is possible to ensure the formation of monodispersed and size-controlled ANPs by combining the seeded growth approach with the coreduction technique using sodium citrate as a reducing agent. Since reduction at high temperature can induce undesired nucleation, great care must be taken to control the seed−Au−Ag−citrate ratio. A metal monomer will be more likely to grow over an existing seed rather that forming a new nucleus if the seed concentration is high. Therefore, it is preferable to use a high seed to metal ion concentration. However, this limits the final size of the particles. For large NP sizes, a multistep approach for particle growth must be used.

Our method relies on the growth of an alloy shell over small Au seed NPs. These seeds are produced using the Turkevich approach, which yields monodispersed small NPs. In principle, Ag or even AuAg alloy seeds could be used instead of Au NPs. We chose to use Au NPs because they are more stable and easier to produce. The presence of a small Au seed at the center does not significantly affect the optical properties of the ANP for a diameter larger than ∼50 nm. Even at ∼30 nm, the theoretical plasmon peak position is only slightly shifted (∼4 nm) but the peak is broader (see Supporting Information, Figure S1). Figure 1 shows the schematics of alloy shell growth on the Au seeds. The resulting ANPs can be used as seeds for subsequent alloy growth, and the process is repeated until the desired size is reached.

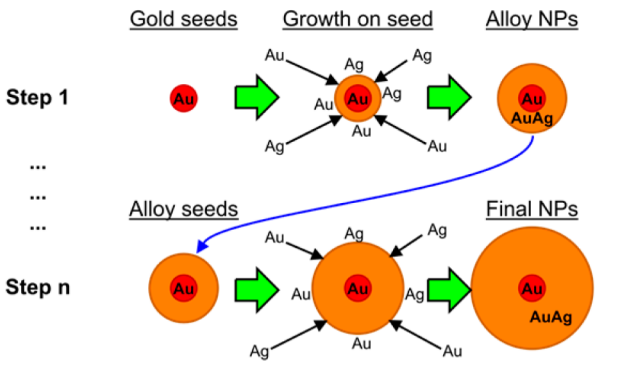

Figure 1. Schematic of the multistep seeded growth synthesis of ANPs. In the first step, monodispersed Au NPs are used as seeds to grow the thick alloy shell. The resulting ANPs are used as seeds for the subsequent growth step, and the process is repeated until the desired size is reached. The composition and size of the ANPs are determined by the Au and Ag concentrations in the suspension.

EXPERIMENTAL METHODS

All reagents used in the synthesis were purchased from Sigma-Aldrich. The 18 MΩ·cm deionized (DI) water is provided by an EMD Millipore Direct-Q 3 ultrapure water purification system. All glassware was cleaned with aqua regia before particle growth to remove any residual metal from previous synthesis and then rinsed thoroughly with DI water.

Au Seed Synthesis. Synthesis of the Au seed particles was made using a standard Turkevich approach.[23] Briefly, 300 μL of a $HAuCl_4$ solution (30 mM) was added to 28 mL of DI water (18 MΩ·cm) in an Erlenmeyer flask and heated to ebullition (100 °C). While stirring the solution, 200 μL of trisodium citrate solution (170 mM) was added rapidly. After a few seconds, the solution becomes transparent before gradually turning to purple and then ruby red. The solution is left heating and stirring for 30 min to ensure complete reduction of the Au ions on the NPs. After the process, DI water is added to the solution in order to adjust the total volume to 30 mL. This synthesis method results in a suspension of particles with a diameter of 15 ± 1 nm and a metallic concentration of 300 μM.

Seeded Growth Synthesis. For a given growth step, the final size of the NPs depends on a parameter that we will call the "seeding ratio" (S_r). It is calculated by dividing the number of Au and Ag atoms in the final suspension of ANPs (alloy shell + initial seed particle) by the number of metal atoms from the seed particles. The S_r is the metric that is used in this paper to characterize the seeded growth steps. Assuming complete reduction and deposition of the Au and Ag ions on the seed particles and assuming that they are distributed equally on all the seeds, S_r is also equal to the ratio of the volumes of the final particle V_f and the seed particle V_{seed}; therefore

DOI: 10.1021/acs.jpcc.5b02728
J. Phys. Chem. C XXXX, XXX, XXX−XXX

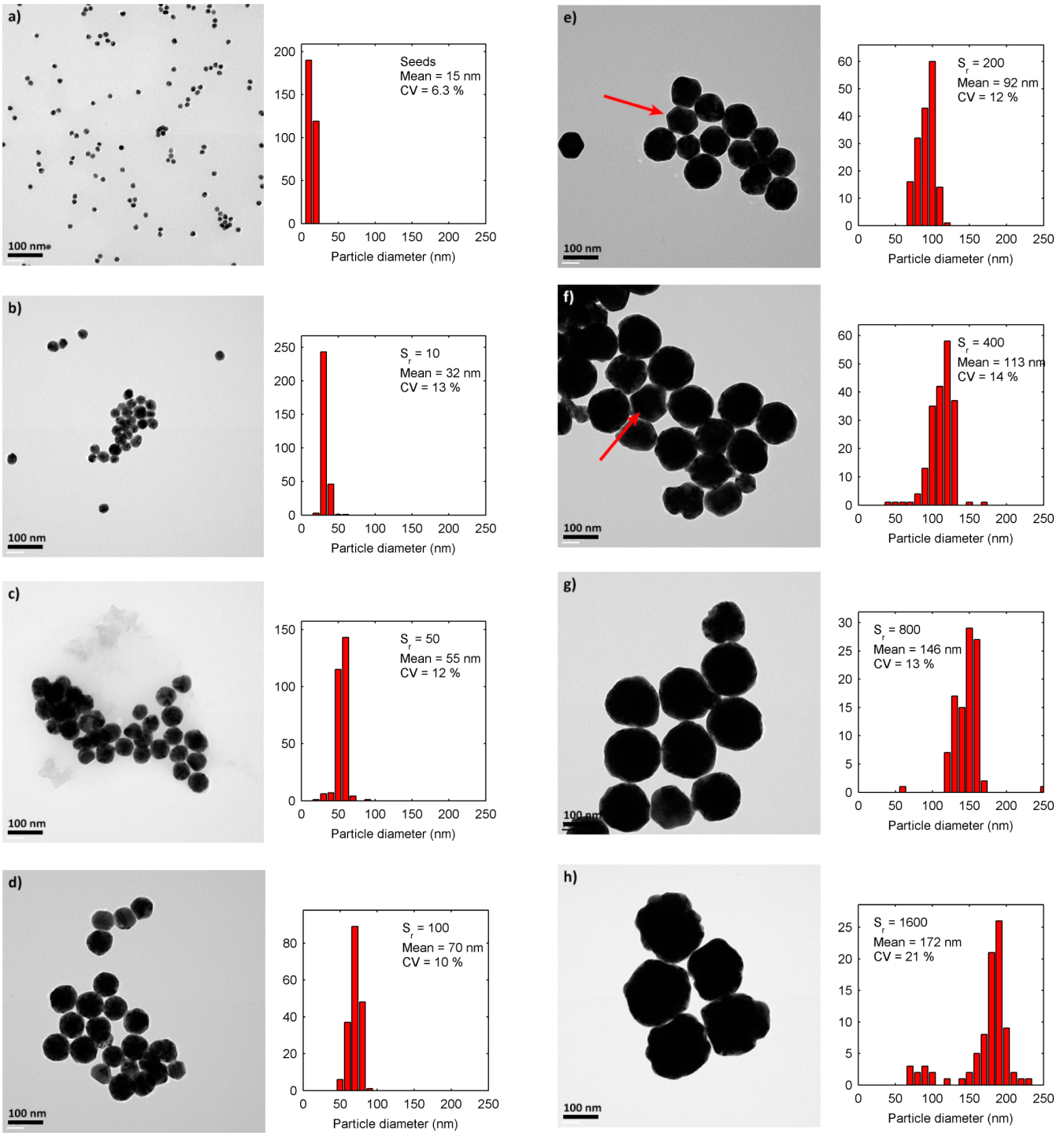

Figure 2. TEM images and the corresponding size distributions for (a) Au seed particles and for AuAg 50:50 ANPs produced in multistep seeded growth using different *Total-*S_r: (b) 10, (c) 50, (d) 100, (e) 200, (f) 400, (g) 800, and (h) 1600.

$$S_r = \frac{V_f}{V_{seed}} = \frac{D^3}{d_0^3} \quad (1)$$

where D and d_0 are the diameters of the final and seed particles, respectively. The final diameter D of the NPs can be deduced from eq 1

$$D = d_0 S_r^{1/3} \quad (2)$$

For NPs produced in a multistep growth, it is important to distinguish between the Seeding ratio relative to the initial Au seeds, which we will call *Total-*S_r, and the seeding ratio of a given growth step, which we will call *Step-*S_r, and for which the seed particle can be a ANP from a previous growth step. The *Total-*S_r for a particle is therefore the product of the *Step-*S_r of all steps used for its production.

Seeded Synthesis of Size-Controlled 50:50 ANPs. ANPs are synthesized by adding $HAuCl_4$ and $AgNO_3$ to a dilute suspension of seeds, growing an alloy shell on the seeds. The ratio of $HAuCl_4$ and $AgNO_3$ determines the final composition of the alloy shell. The total metallic concentration

DOI: 10.1021/acs.jpcc.5b02728
J. Phys. Chem. C XXXX, XXX, XXX−XXX

(seeds + Au and Ag salts) is 150 μM. A predetermined amount of seeds (for the desired seeding ratio) is added to DI water and heated to ebullition in a three-necked round-bottom flask placed in a water heat bath with refluxing. The total volume of seed suspension and DI water is about 95 mL. At ebullition and with constant stirring (550 rpm), predetermined volumes of $HAuCl_4$ (30 mM) and $AgNO_3$ (30 mM) solution are added simultaneously to the water. Immediately after, 1 mL of trisodium citrate solution (170 mM) is added to the solution. The solution is then left heating and stirring for 60 min to complete the reaction. The total volume is then adjusted to 100 mL with DI water.

For example, the synthesis of 50:50 ANPs with *Total*-S_r = 10 was accomplished by adding 5 mL of the seed suspension into 90 mL of boiling DI water with constant stirring. Afterward, 225 μL of $HAuCl_4$ and 225 μL of $AgNO_3$ were added simultaneously to the boiling solution followed immediately by 900 μL of the trisodium citrate solution. For information on the amount of reagents used for the other samples, see Table 1 in the Supporting Information.

Synthesis of Composition-Controlled ANPs. In this case, the ANPs were synthesized using the method presented above using two sequential steps: (i) the first step uses the small Au NPs as seeds with a *Total*-S_r = 10, and (ii) the second step uses the particles synthesized in the first step as seeds with a *Step*-S_r = 10 again, resulting in a *Total*-S_r = 100 between the final particles and the initial Au seeds. For each step, the volumes of Au and Ag precursor solutions are adjusted for the desired final alloy composition. For this experiment, ANPs with compositions ranging from pure Au to pure Ag in 10% Ag composition increments were synthesized.

For example, the synthesis of 20:80 AuAg ANPs with *Total*-S_r = 10 was accomplished by adding 5 mL of the seed suspension into 90 mL of DI water heated to ebullition with constant stirring. Afterward, 90 μL of $HAuCl_4$ and 360 μL of $AgNO_3$ were added simultaneously to the boiling solution followed immediately by 900 μL of the trisodium citrate solution. The final volume was adjusted to 100 mL with DI water.

Afterward, the 20:80 AuAg ANPs with *Total*-S_r = 100 were synthesized by adding 10 mL of the previous suspension into 85 mL of DI water heated to ebullition with constant stirring. Then 90 μL of $HAuCl_4$ and 360 μL of $AgNO_3$ were added simultaneously to the boiling solution followed immediately by 900 μL of the trisodium citrate solution. The final volume was adjusted to 100 mL with DI water. For information on the amount of reagents used for the other samples, see Tables 2 and 3 in the Supporting Information.

Characterization of the Samples. Extinction spectra were measured using a multiplate spectrophotometer (BioTek, Epoch). Imaging of the NPs was performed using a TEM (JEM-2100F, JEOL) with a 200 kV accelerating voltage. For the TEM sample preparation, 5 μL of the samples was dropped on a 400 mesh copper grid coated with a thin carbon film (Cu-400CN, Pacific grid tech) and dried before imaging. This TEM is also equipped with an X-ray detector to perform EDS in order to measure the composition of the ANPs. The electron beam diameter was 1 nm for the point composition measurements.

RESULTS AND DISCUSSION

Seeded Synthesis of Size-Controlled ANPs. Figure 2 shows transmission electron microscope (TEM) images and the size distributions measured for the Au seed NPs as well as the 50:50 ANPs with increasing sizes. All of these NPs were synthesized using multistep growth where the particles with *Total*-S_r = 10 were used as seeds for particles with *Total*-S_r = 50, which in turn were used as seeds for particles *Total*-S_r = 100 and so on. Although the CV for the ANPs is not as low as the initial Au seeds (6.3%), it remains under 15% for all samples except for the largest particles (*Total*-S_r = 1600). In this case, the larger CV is caused by the presence of a smaller NP population in the 50−100 nm range, which is likely caused by nucleation of new particles during the growth process. Indeed, for a similar metallic concentration, large particles have less total surface area available for growth, resulting in a slower growth and the possibility for new nucleation.[29]

The majority of these particles are spherical or slightly ellipsoid, and no elongated or "nanorod" like NPs were observed. Few particles show some facets with a slightly hexagonal or triangular shape (some examples are indicated by red arrows on Figure 2e and 2f), but their relative abundance is very low (<5% of NPs), and they likely have a negligible effect on the suspension color or extinction spectrum. It is interesting to note that such nonspherical NPs also exist in the initial Au seeds and are probably the origin of those nonspherical ANPs.

Because of the narrow size distributions, it is expected that the mean ANP sizes of our samples will follow eq 2. Indeed, Figure 3 shows that the mean size of the particles is linear with

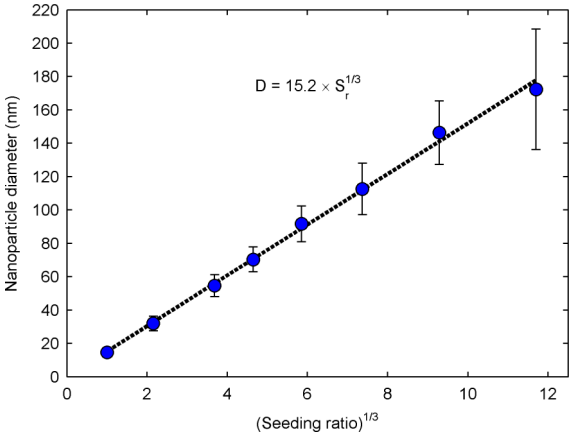

Figure 3. Mean NP diameter showing a linear relationship with the cubic root of *Total*-S_r. Linear regression is used to compute the slope, which corresponds to the mean diameter of the Au seeds. Vertical error bars represent one standard deviation as measured by TEM. The first point represents the Au seeds, and the other points represent ANPs with 50:50 alloy shell composition.

$S_r^{1/3}$. According to eq 2, the slope corresponds to the diameter of the initial seed particles. In this case, the slope indicates particles of 15.2 nm, in good agreement with the 15 ± 1 nm mean diameter measured by TEM for the Au seeds (Figure 2a).

Synthesis of Composition-Controlled ANPs. It is easy to produce ANPs with different compositions simply by changing the ratio of Au and Ag precursor salts during synthesis. Figure 4 shows the variation in the color of the transmitted light with the variation of the alloy composition for ANPs. The ANPs suspension color varies from red to yellow with increasing Ag content.

An average size around 66 nm with a 15% CV was measured by TEM. According to EDS measurements over many ANPs, the average gold molar fraction (GMF) is within 3 atom % of the expected value, with a standard deviation from particle to

DOI: 10.1021/acs.jpcc.5b02728
J. Phys. Chem. C XXXX, XXX, XXX−XXX

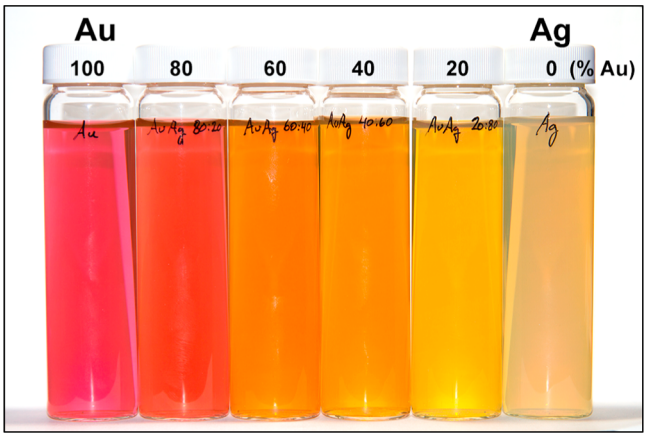

Figure 4. Photograph of the ANPs suspensions showing the effect of alloy composition on the color of the suspension. From left to right: Au, AuAg 80:20, AuAg 60:40, AuAg 40:60, AuAg 20:80, and Ag suspensions prepared by a two-step growth with a *Total-S*$_r$ = 100, which corresponds to NPs with a 66 nm mean diameter.

particle of 7 atom % or less (see Supporting Information, Figure S2), which is similar to values measured for ANPs generated by laser ablation.[30] The variation in the color of the transmitted light is due to the shifting of the extinction peak with composition. The theoretical extinction spectra of the NPs in water were computed with Mie theory,[31] adapted for the treatment of coated spheres,[32] using modeled composition-dependent dielectric functions for the AuAg alloy material.[33] Calculations for the plasmon peak position as a function of composition were done assuming a 15 nm Au seed core diameter and a homogeneous alloy shell with a 66 nm mean outer diameter and a 15% CV. Figure 5 shows the measured extinction spectra for ANPs with gold molar fractions (GMF) of the alloy shell varying from 0 to 100% in 10% increments and comparison with the corresponding calculated extinction spectra. Both the measured peak positions and the half-widths half-maximum (HWHM, defined as the difference between the wavelength at the peak maximum and the wavelength at which its value has dropped to one-half of the maximum value) agree well with the calculated values, except for a slight difference in the peak position at low Au concentration and the HWHM for pure Ag. The extinction peak for pure Ag NPs is notably broader than for the other alloy compositions. For Ag, the citrate reduction technique is known to produce less spherical particles with a broader size distribution.[34] It is interesting to note that the particles have a narrower peak for the alloys. This could be due to the interaction of Au and Ag atoms producing more spherical particles.[35] Long-term stability of the ANPs is very good, with no visible aggregation of the particles and only a small red shift of the extinction peak position (<5 nm) after 1 year.

Evaluation of Alloy Shell Homogeneity. The synthesis of ANPs by chemical reduction can lead to nonhomogeneous alloy formation, with a Au-rich core and a Ag-rich surface.[18,19] For further understanding of the composition profile of the ANPs synthesized by seeded growth, the spatial alloy composition was measured by energy-dispersive X-ray spectroscopy (EDS) in a TEM on many ANPs. Figure 6 shows a representative example of the measured atomic compositions of Au and Ag at different points of a 28 nm ANP with a 50:50 alloy shell composition and the measured extinction spectrum of the corresponding ANPs suspension. For this particle, the

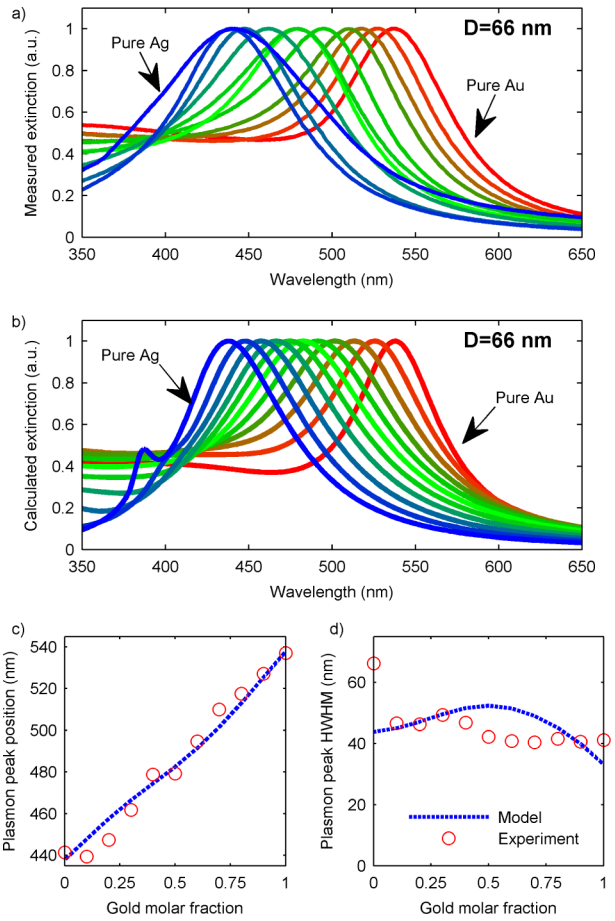

Figure 5. (a) Measured and (b) calculated extinction spectra of ANPs with shell compositions varying from pure Au to pure Ag in 10% GMF increments. Agreement between (c) the measured and the calculated plasmon peak positions and (d) the measured and the calculated plasmon peak HWHM. ANPs were synthesized with a *Total-S*$_r$ = 100.

overall composition was measured to be within 2% of the expected 55:45 AuAg composition (the pure Au core represents 10% of the particle volume; the remaining 90% is the 50:50 alloy shell). As expected from the literature, we observed an Ag-rich surface with an Au-rich core. Although the simple presence of an Au seed at the core of the particle explains the higher Au content measured at the center of the particle, the Ag-rich surface can only be explained by an inhomogeneous alloy composition in the shell; otherwise, the measurement would have been 50:50 at these points.

Since the composition is not homogeneous, it is important to understand the effect on the optical properties. Most ANPs present a symmetrical plasmon peak. However, for small (~30 nm) ANPs produced by the seeded growth coreduction technique presented here, the measured extinction spectrum is nonsymmetric (see Figure 6b). The theoretical extinction spectrum calculated by Mie theory for a 28 nm diameter ANP with a homogeneous 50:50 alloy shell should be symmetrical (green line, Figure 6b). The nonsymmetrical extinction spectrum probably results from the not homogeneous alloy composition, with a GMF dependent on the radial position.

Mie theory can only account for discrete volumes, each of which has a homogeneous composition. The effect of nonhomogeneous alloy shell was computed by modeling the ANPs as a 13 nm Au seed core with 50 concentric

DOI: 10.1021/acs.jpcc.5b02728
J. Phys. Chem. C XXXX, XXX, XXX−XXX

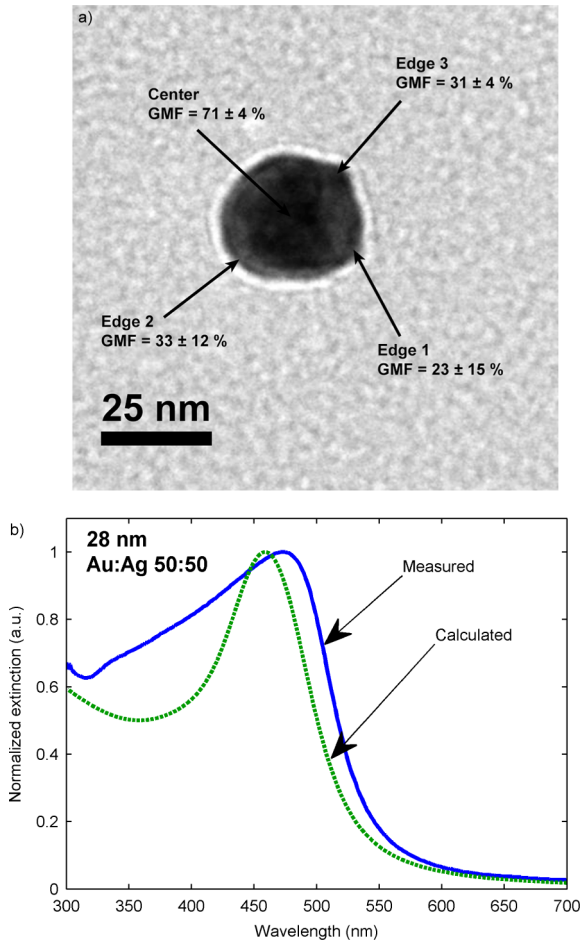

Figure 6. (a) Alloy composition measured by EDS at different points in the 50:50 ANP. The core is Au rich, whereas the surface of the particle is Ag rich. (b) Measured and calculated extinction spectra for the corresponding ANP suspension. The measured peak is much broader and asymmetrical relative to the theoretically expected one.

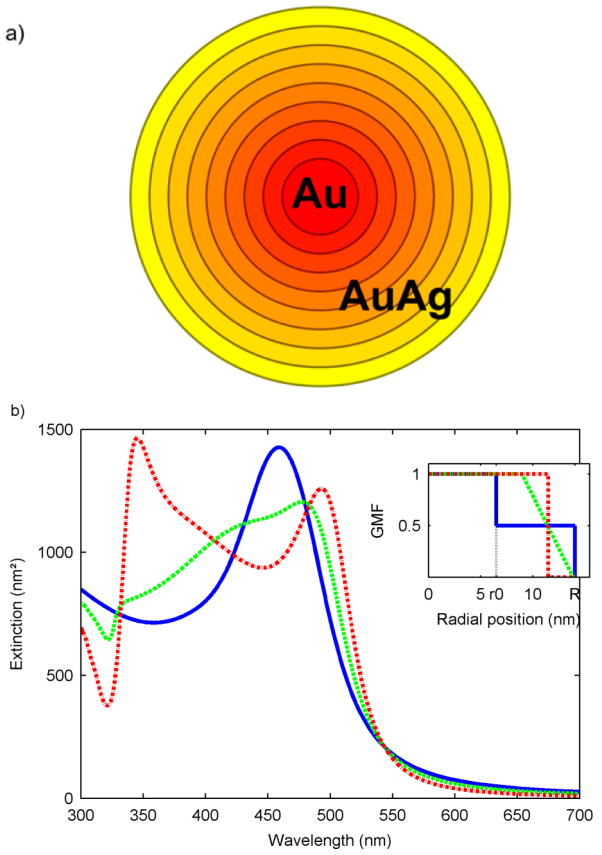

Figure 7. (a) Schematic of the modeling of inhomogeneous alloy shell composition with concentric shells of homogeneous compositions. (b) Calculated extinction spectra for the ideal case of a homogeneous profile (slope = 0, blue line), a linear profile (green line), and a core–shell structure (infinite slope, red line), showing the effect of the average composition slope on the extinction spectrum. (Inset) Corresponding radial composition profiles. In this example, r_0 = 7.5 nm and R = 14 nm are the radii of the Au seed and the ANP, respectively.

homogeneous alloy shells of equal thicknesses but varying compositions, as represented schematically in Figure 7a. The composition profile was controlled so that the overall mean shell composition was equal to that of the experimental ANPs.

The measured extinction spectrum was fitted by assuming a quadratic dependence of the GMF on the radial position. Although the initial fitting algorithm permitted a quadratic dependence, it converged to an almost linear dependence, with a higher Au content near the Au core and an Ag-rich surface. As it turns out, the linear term is the most important; the second-order coefficient only slightly affects the extinction spectrum (see Supporting Information, Figure S3). For this reason and for the sake of simplicity, we fitted the radial composition dependence using a simple linear fit. It should be noted that the fitting algorithm prevented unphysical values of GMF by restricting its values between 0 and 1. It also restricted the average composition of the shell to a fixed composition (50% Au in this case).

Because of the restriction on the average shell composition, the linear model that was used for fitting the peaks has only one degree of liberty: the slope of the composition profile. Figure 7b shows how the slope affects the shape and width of the plasmon peak in the case of a homogeneous shell (zero slope, blue line), a linear profile (nonzero slope, green line), and a core–shell profile (infinite slope, red line). For a zero slope, the peak is symmetrical and the narrowest. As the slope increases, the peak broadens and loses symmetry until the slope becomes infinite and the structure becomes that of an AuAg core–shell. In this case, the extinction spectrum shows two distinct peaks.

Figure 8 shows the good agreement using this fitted composition dependence compared to the measured spectrum. As observed for small NPs (28 nm), the extinction peak is broad and nonsymmetrical but can be modeled accurately by simple linear composition dependence (Figure 8a). For larger NPs (60 nm), the measured extinction peak is symmetrical but slightly broader than the theoretical peak for homogeneous alloy shell (Figure 8b). Using a similar fit with linear composition dependence, the measured peak can be modeled very accurately.

Although peak asymmetry broadens the plasmon peak, which has a detrimental effect in many applications requiring narrow peaks, it is interesting to note that this effect is only important for small particles (<50 nm). Therefore, for applications that require large NPs, the inhomogeneous composition has an almost negligible effect on the plasmon peak, and thus, it is not a necessity to synthesize ANPs with homogeneous composition. Furthermore, for large NPs, alloy inhomogeneity can be neglected in the calculation of the optical properties. Therefore,

DOI: 10.1021/acs.jpcc.5b02728
J. Phys. Chem. C XXXX, XXX, XXX–XXX

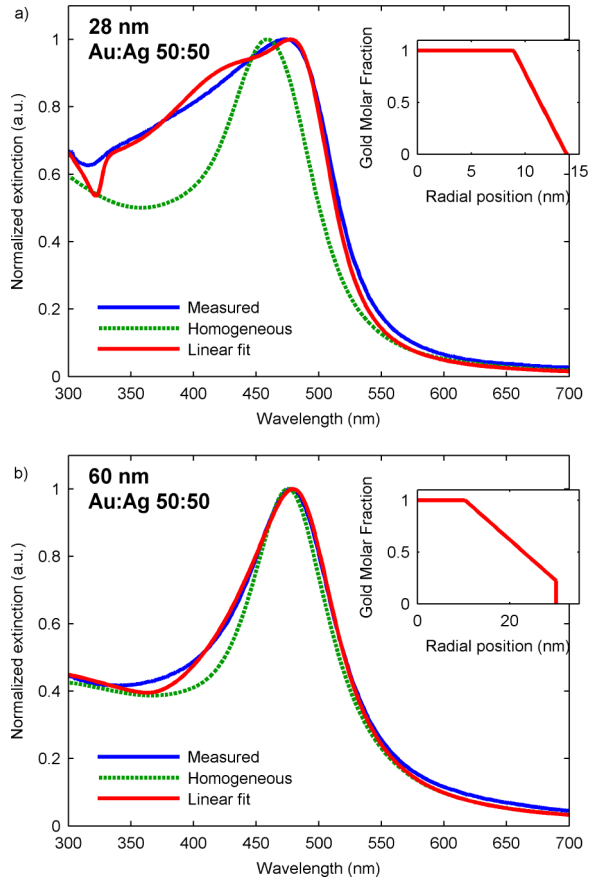

Figure 8. Comparison of the measured (blue line) and theoretical extinction spectra for homogeneous (green line) and linear fit of the alloy composition (red line) for (a) 28 and (b) 60 nm ANPs with a 50:50 alloy shell. (Insets) Radial GMF fitted in each case.

the results presented in Figure 5 remain valid even if the alloy shell was considered homogeneous.

The Ag-rich surface is probably caused by the galvanic replacement of Ag atoms at the NP surface by Au ions during particle growth. Because of the higher reduction potential of Au compared to Ag, Au^{3+} ions can oxidize Ag^0 atoms at the particle surface to Ag^+ ions, leading to their release into the solution and the Au^{3+} ions being reduced to Au^0 at the particle surface, according to the following reaction[10,13]

$$Au^{3+}(aq) + 3Ag^0(S) \rightarrow Au^0(S) + 3Ag^+(aq) \quad (3)$$

This phenomenon is used, for example, to produce hollow Au NPs from Ag NPs[36] or Au nanocages from Ag nanocubes.[37,38] In our case, hollow NPs are not formed because the reduction by citrate is taking place simultaneously and continuously adds Au and Ag atoms to fill the vacancies. However, the galvanic replacement leads to a higher net growth rate of Au and a lower net growth rate of Ag at the beginning of alloy shell growth. This phenomenon results in a gradual increase of the Ag to Au ratio into the solution during growth, explaining the higher Au concentration near the seed and the Ag-rich surface (see Figure 9).

CONCLUSION

We developed a synthesis method for AuAg ANPs with controlled size and composition using a combination of coreduction and seeded growth. Compared to other methods limited to ANPs with a ~30 nm diameter, our seeded growth approach produces ANPs with a size that can be controlled between ~30 and ~150 nm with a CV of less than 15%, indicating a highly monodisperse suspension. The alloy shell composition of these ANPs is not homogeneous and can significantly affect the extinction peak for small ANPs (<30 nm), but this effect is negligible for larger ANPs (>60 nm).

Due to their composition-controlled plasmon peak, such ANPs present great interest in multiplexed biological imaging.[20] The larger NPs (>50 nm) are especially interesting because of their strong scattering.

ASSOCIATED CONTENT

Supporting Information

Effect of Au core on the optical properties; measurements of ANP size and composition distributions; comparison between linear and quadratic composition profiles; amount of reagents used for the various ANP syntheses. The Supporting

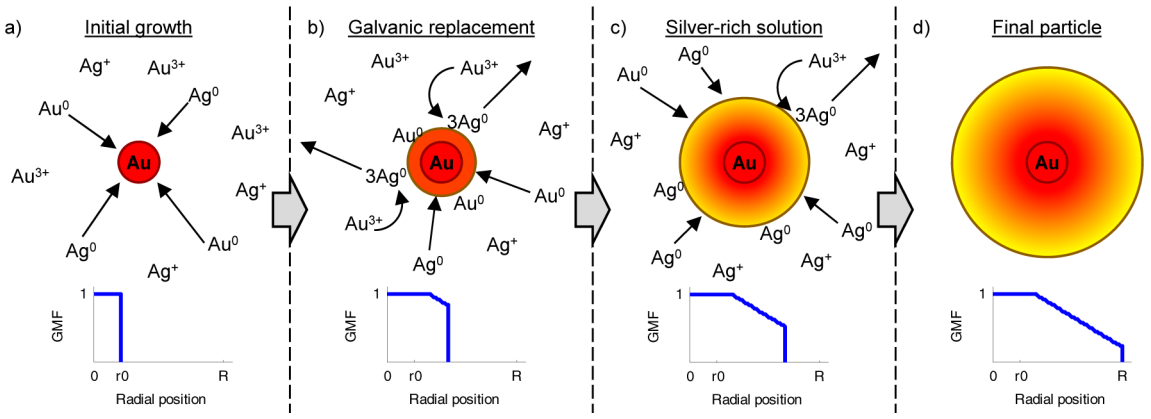

Figure 9. Schematic view of the growth mechanism for the example of a 50:50 alloy shell, explaining the Au-rich core and the Ag-rich surface. (a) Au and Ag ions are initially at the same concentration in the solution, and both grow on the seed surface. (b) After the initial deposition of Au and Ag atoms, Au^{3+} ions in the solution can oxidize and replace Ag atoms at the surface by the galvanic replacement reaction (curved arrows), resulting in a higher net deposition of Au relative to Ag, which explains the observed higher Au content near the seed. (c) Later in the growth, the remaining ions in the solution are mostly Ag ions, explaining the Ag-rich surface of the final particle (d). (Insets) Schematic view of the radial Au composition profile at each represented growth steps.

DOI: 10.1021/acs.jpcc.5b02728
J. Phys. Chem. C XXXX, XXX, XXX−XXX

Information is available free of charge on the ACS Publications website at DOI: 10.1021/acs.jpcc.5b02728.

AUTHOR INFORMATION

Corresponding Author

*Phone: (514) 340-4711 ext. 4971. Fax: (514) 340-3218. E-mail: michel.meunier@polymtl.ca.

Author Contributions

The manuscript was written through contributions of all authors. All authors have given approval to the final version of the manuscript.

Notes

The authors declare no competing financial interest.

ACKNOWLEDGMENTS

We acknowledge the financial contribution of the Natural Sciences and Engineering Research Council of Canada. We also thank J.-P. Masse from the CM^2 at Polytechnique Montréal for his help in the EDS measurements.

ABBREVIATIONS

NP, nanoparticle; ANP, alloy nanoparticle; CV, coefficient of variation; TEM, transmission electron microscope; GMF, gold molar fraction; HWHM, half-width half-maximum; EDS, energy-dispersive X-ray spectroscopy

REFERENCES

(1) Stockman, M. I. Nanoplasmonics: The Physics Behind the Applications. *Phys. Today* **2011**, *64*, 39.

(2) Garcia, M. A. Surface Plasmons in Metallic Nanoparticles: Fundamentals and Applications. *J. Phys. D: Appl. Phys.* **2011**, *44*, 283001.

(3) Jain, P. K.; Lee, K. S.; El-Sayed, I. H.; El-Sayed, M. A. Calculated Absorption and Scattering Properties of Gold Nanoparticles of Different Size, Shape, and Composition: Applications in Biological Imaging and Biomedicine. *J. Phys. Chem. B* **2006**, *110*, 7238−7248.

(4) Murphy, C. J.; Sau, T. K.; Gole, A. M.; Orendorff, C. J.; Gao, J.; Gou, L.; Hunyadi, S. E.; Li, T. Anisotropic Metal Nanoparticles: Synthesis, Assembly, and Optical Applications. *J. Phys. Chem. B* **2005**, *109*, 13857−13870.

(5) Tiedemann, D.; Taylor, U.; Rehbock, C.; Jakobi, J.; Klein, S.; Kues, W. A.; Barcikowski, S.; Rath, D. Reprotoxicity of Gold, Silver, and Gold-Silver Alloy Nanoparticles on Mammalian Gametes. *Analyst* **2014**, *139*, 931−942.

(6) Besner, S.; Meunier, M. Femtosecond Laser Synthesis of AuAg Nanoalloys: Photoinduced Oxidation and Ions Release. *J. Phys. Chem. C* **2010**, *114*, 10403−10409.

(7) Radziuk, D. V.; Zhang, W.; Shchukin, D.; Möhwald, H. Ultrasonic Alloying of Preformed Gold and Silver Nanoparticles. *Small* **2010**, *6*, 545−553.

(8) Peng, Z.; Spliethoff, B.; Tesche, B.; Walther, T.; Kleinermanns, K. Laser-Assisted Synthesis of Au-Ag Alloy Nanoparticles in Solution. *J. Phys. Chem. B* **2006**, *110*, 2549−2554.

(9) Grade, S.; Eberhard, J.; Jakobi, J.; Winkel, A.; Stiesch, M.; Barcikowski, S. Alloying Colloidal Silver Nanoparticles with Gold Disproportionally Controls Antibacterial and Toxic Effects. *Gold Bull.* **2014**, *47*, 83−93.

(10) Gonzalez, C. M.; Liu, Y.; Scaiano, J. C. Photochemical Strategies for the Facile Synthesis of Gold-Silver Alloy and Core-Shell Bimetallic Nanoparticles. *J. Phys. Chem. C* **2009**, *113*, 11861−11867.

(11) Liu, S.; Chen, G.; Prasad, P. N.; Swihart, M. T. Synthesis of Monodisperse Au, Ag, and Au-Ag Alloy Nanoparticles with Tunable Size and Surface Plasmon Resonance Frequency. *Chem. Mater.* **2011**, *23*, 4098−4101.

(12) Zhang, Q.; Xie, J.; Liang, J.; Lee, J. Y. Synthesis of Monodisperse Ag-Au Alloy Nanoparticles with Independently Tunable Morphology, Composition, Size, and Surface Chemistry and Their 3-D Superlattices. *Adv. Funct. Mater.* **2009**, *19*, 1387−1398.

(13) Shore, M. S.; Wang, J.; Johnston-Peck, A. C.; Oldenburg, A. L.; Tracy, J. B. Synthesis of Au(Core)/Ag(Shell) Nanoparticles and Their Conversion to AuAg Alloy Nanoparticles. *Small* **2011**, *7*, 230−234.

(14) Rodríguez-González, B.; Burrows, A.; Watanabe, M.; Kiely, C. J.; Liz Marzán, L. M. Multishell Bimetallic AuAg Nanoparticles: Synthesis, Structure and Optical Properties. *J. Mater. Chem.* **2005**, *15*, 1755.

(15) Link, S.; Wang, Z. L.; El-Sayed, M. A. Alloy Formation of Gold−Silver Nanoparticles and the Dependence of the Plasmon Absorption on Their Composition. *J. Phys. Chem. B* **1999**, *103*, 3529−3533.

(16) Sánchez-Ramírez, J. F.; Pal, U.; Nolasco-Hernández, L.; Mendoza-Álvarez, J.; Pescador-Rojas, J. A. Synthesis and Optical Properties of Au-Ag Alloy Nanoclusters with Controlled Composition. *J. Nanomater.* **2008**, *2008*, 1−9.

(17) Mallin, M. P.; Murphy, C. J. Solution-Phase Synthesis of Sub-10 Nm Au−Ag Alloy Nanoparticles. *Nano Lett.* **2002**, *2*, 1235−1237.

(18) Mahl, D.; Diendorf, J.; Ristig, S.; Greulich, C.; Li, Z.-A.; Farle, M.; Köller, M.; Epple, M. Silver, Gold, and Alloyed Silver−gold Nanoparticles: Characterization and Comparative Cell-Biologic Action. *J. Nanopart. Res.* **2012**, *14*, 1153.

(19) Li, T.; Albee, B.; Alemayehu, M.; Diaz, R.; Ingham, L.; Kamal, S.; Rodriguez, M.; Bishnoi, S. W. Comparative Toxicity Study of Ag, Au, and Ag-Au Bimetallic Nanoparticles on Daphnia Magna. *Anal. Bioanal. Chem.* **2010**, *398*, 689−700.

(20) Patskovsky, S.; Bergeron, E.; Rioux, D.; Simard, M.; Meunier, M. Hyperspectral Reflected Light Microscopy of Plasmonic Au/Ag Alloy Nanoparticles Incubated as Multiplex Chromatic Biomarkers with Cancer Cells. *Analyst* **2014**, *139*, 5247−5253.

(21) Patskovsky, S.; Bergeron, E.; Rioux, D.; Meunier, M. Wide-Field Hyperspectral 3D Imaging of Functionalized Gold Nanoparticles Targeting Cancer Cells by Reflected Light Microscopy. *J. Biophotonics* **2014**, DOI: 10.1002/jbio.201400025.

(22) Patskovsky, S.; Bergeron, E.; Meunier, M. Hyperspectral Darkfield Microscopy of PEGylated Gold Nanoparticles Targeting CD44-Expressing Cancer Cells. *J. Biophotonics* **2013**, *6*, 1−6.

(23) Turkevich, J.; Stevenson, P. C.; Hillier, J. A Study of the Nucleation and Growth Processes in the Synthesis of Colloidal Gold. *Discuss. Faraday Soc.* **1951**, *11*, 55.

(24) Frens, G. Controlled Nucleation for the Regulation of the Particle Size in Monodisperse Gold Suspensions. *Nat. Phys. Sci.* **1973**, *241*, 20−22.

(25) Ji, X.; Song, X.; Li, J.; Bai, Y.; Yang, W.; Peng, X. Size Control of Gold Nanocrystals in Citrate Reduction: The Third Role of Citrate. *J. Am. Chem. Soc.* **2007**, *129*, 13939−13948.

(26) Brown, K. R.; Natan, M. J. Hydroxylamine Seeding of Colloidal Au Nanoparticles in Solution and on Surfaces. *Langmuir* **1998**, *14*, 726−728.

(27) Brown, K. R.; Walter, D. G.; Natan, M. J. Seeding of Colloidal Au Nanoparticle Solutions. 2. Improved Control of Particle Size and Shape. *Chem. Mater.* **2000**, *12*, 306−313.

(28) Perrault, S. D.; Chan, W. C. W. Synthesis and Surface Modification of Highly Monodispersed, Spherical Gold Nanoparticles of 50−200 nm. *J. Am. Chem. Soc.* **2009**, *131*, 17042−17043.

(29) Ziegler, C.; Eychmüller, A. Seeded Growth Synthesis of Uniform Gold Nanoparticles with Diameters of 15−300 nm. *J. Phys. Chem. C* **2011**, *115*, 4502−4506.

(30) Neumeister, A.; Jakobi, J.; Rehbock, C.; Moysig, J.; Barcikowski, S. Monophasic Ligand-Free Alloy Nanoparticle Synthesis Determinants during Pulsed Laser Ablation of Bulk Alloy and Consolidated Microparticles in Water. *Phys. Chem. Chem. Phys.* **2014**, *16*, 23671−23678.

(31) Mie, G. Beiträge Zur Optik Trüber Medien, Speziell Kolloidaler Metallösungen. *Ann. Phys.* **1908**, *330*, 377−445.

DOI: 10.1021/acs.jpcc.5b02728
J. Phys. Chem. C XXXX, XXX, XXX−XXX

(32) Le Ru, E. C.; Etchegoin, P. G. *Principles of Surface-Enhanced Raman Spectroscopy and Related Plasmonic Effects*; Elsevier: Amsterdam, 2009.
(33) Rioux, D.; Vallières, S.; Besner, S.; Muñoz, P.; Mazur, E.; Meunier, M. An Analytic Model for the Dielectric Function of Au, Ag, and Their Alloys. *Adv. Opt. Mater.* **2014**, *2*, 176−182.
(34) Wan, Y.; Guo, Z.; Jiang, X.; Fang, K.; Lu, X.; Zhang, Y.; Gu, N. Quasi-Spherical Silver Nanoparticles: Aqueous Synthesis and Size Control by the Seed-Mediated Lee-Meisel Method. *J. Colloid Interface Sci.* **2013**, *394*, 263−268.
(35) Xia, H.; Bai, S.; Hartmann, J.; Wang, D. Synthesis of Monodisperse Quasi-Spherical Gold Nanoparticles in Water via silver(I)-Assisted Citrate Reduction. *Langmuir* **2010**, *26*, 3585−3589.
(36) Fairbairn, N.; Christofidou, A.; Kanaras, A. G.; Newman, T. A; Muskens, O. L. Hyperspectral Darkfield Microscopy of Single Hollow Gold Nanoparticles for Biomedical Applications. *Phys. Chem. Chem. Phys.* **2013**, *15*, 4163−4168.
(37) Skrabalak, S. E.; Chen, J.; Au, L.; Lu, X.; Li, X.; Xia, Y. Gold Nanocages for Biomedical Applications. *Adv. Mater.* **2007**, *19*, 3177−3184.
(38) Chen, J.; McLellan, J. M.; Siekkinen, A.; Xiong, Y.; Li, Z.-Y.; Xia, Y. Facile Synthesis of Gold-Silver Nanocages with Controllable Pores on the Surface. *J. Am. Chem. Soc.* **2006**, *128*, 14776−14777.

DOI: 10.1021/acs.jpcc.5b02728
J. Phys. Chem. C XXXX, XXX, XXX−XXX